*Psychophysiology, 00* (2015), 00–00. Wiley Periodicals, Inc. Printed in the USA.

DOI: 10.1111/psyp.12519

# The neural correlates of motion-induced shifts in reaching

BORJA RODRÍGUEZ-HERREROS,[a,b,c] ANTONI RODRÍGUEZ-FORNELLS,[a,b,d] AND JOAN LÓPEZ-MOLINER[a,e]

[a]Department of Basic Psychology, Universitat de Barcelona, Barcelona, Spain
[b]Cognition and Brain Plasticity Group, Bellvitge Biomedical Research Institute–IDIBELL, Barcelona, Spain
[c]LREN and Service de Génetique Médicale, Centre Hospitalier Universitaire Vaudois, Lausanne, Switzerland
[d]Catalan Institution for Research and Advanced Studies, ICREA, Barcelona, Spain
[e]Institute for Brain, Cognition and Behavior (IR3C), Universitat de Barcelona, Barcelona, Spain

**Abstract**

A basic function of the visual system is to estimate the location of objects. Among other sensory inputs, the coding of an object's position involves the integration of visual motion, such as that produced by other moving patterns in the scene. Psychophysical evidence has shown that motion signals can shift, in the direction of motion, both the perceived position and the directed action to a stationary object. The neural mechanisms that sustain this effect are generally assumed to be mediated by feedback circuits from the middle temporal area to the primary visual cortex. However, evidence from neural responses is lacking. We used measures of ERPs and Granger causality analysis—a tool to predict the causal connectivity of two brain responses—to unravel the circuit by which motion influences position coding. We found that the motion-induced hand shift is tightly related to a neural delay: Participants with larger shifts of the pointing location presented slower sensory processing, in terms of longer peak latencies of the primary visual evoked potentials. We further identified early neural activity in the vicinity of the extrastriate cortex as the cause of this delay, which likely reflects the early processing of motion signals in position coding. These results suggest the rapid transfer of visual motion through feedforward circuits as a putative neural substrate in charge of the motion-induced shift in reaching.

**Descriptors:** Reaching, Position coding, Extrastriate cortex, Feedforward circuits

Object localization is a challenging task for the visual system. Numerous psychophysical studies indicate that position coding depends not only on the retinal location (Bock, 1986) and eye movements (Cai, Pouget, Schlag-Rey, & Schlag, 1997), but also on nearby motion (Snowden, 1998). A particularly compelling example occurs when a stationary object is flashed in the vicinity of a moving pattern: The perceived position of and the reaching movement toward the object are biased in the direction of motion (Brenner & Smeets, 1997; De Valois & De Valois, 1991; Nijhawan, 2002; Whitney & Cavanagh, 2000). These shifts indicate that motion-related brain areas, such as the middle temporal area (MT), play a prominent role in position coding (McGraw, Walsh, & Barrett, 2004). Little is known, however, about the neural mechanisms that serve to induce this bias. Animal single-cell recordings described motion-induced shifts in the receptive field properties of retinal, primary visual cortex (V1), and V4 neurons (Berry, Brivanlou, Jordan, & Meister, 1999; Fu, Shen, Gao, & Dan, 2004; Sundberg, Fallah, & Reynolds, 2006). In humans, neuroimaging studies revealed similar changes in the retinotopic representation of stationary flashes in V1 and MT (Maus, Fischer, & Whitney, 2013; Whitney, Goltz et al., 2003). As primary visual areas are therefore involved in position coding, the effects of motion have been traditionally associated to recurrent circuits from area MT to V1 (De Valois & De Valois, 1991; Nishida & Johnston, 1999). Structurally, a rich network of reciprocal projections exists between these two regions, conveying feedback connections to V1 (Shipp & Zeki, 1989). This is done, however, at the cost of adding neural delays that compromise fast recovering of spatial codes, especially in rapid goal-directed actions that are early affected by motion (∼120 ms; Brenner & Smeets, 1997; Whitney, Westwood, & Goodale, 2003).

Here, we investigated the time course of the neural correlates associated with motion-induced shifts in reaching. We explored the possibility that the motion-induced hand shift may be quickly subserved by feedforward connections, before resorting to the MT-V1 reentrant circuit. MT neurons responding to visual stimuli fire almost simultaneously to V1 (∼40–75 ms; Maunsell, 1987; Nowak & Bullier, 1997). It is difficult to assume, therefore, that the earliest MT responses depend on V1 input. Instead, thalamocortical projections might sustain MT short latency (Sincich, Park, Wohlgemuth,

The authors thank T. Cunillera, J. Marco-Pallarés, J. L. Amengual, and A. P. Bellido for helpful discussions and advice on data collection/analysis. Thanks also to D. Linares, E. Johnson, E. Brenner, M. A. Schoenfeld, and Lester Melie-García for comments on the manuscript. This work was supported by an AGAUR B.E. grant from the Catalan government to BRH, Spanish government grants to ARF (PSI2012-29219) and JLM (PSI2013-41568-P), and a grant from the Generalitat de Catalunya (2014SGR-79). JLM was also supported by an ICREA Academia Distinguished Professorship award.

Address correspondence to: Joan López-Moliner, Departament de Psicologia Bàsica, Universitat de Barcelona, 08035 Barcelona, Catalonia, Spain. E-mail: j.lopezmoliner@ub.edu

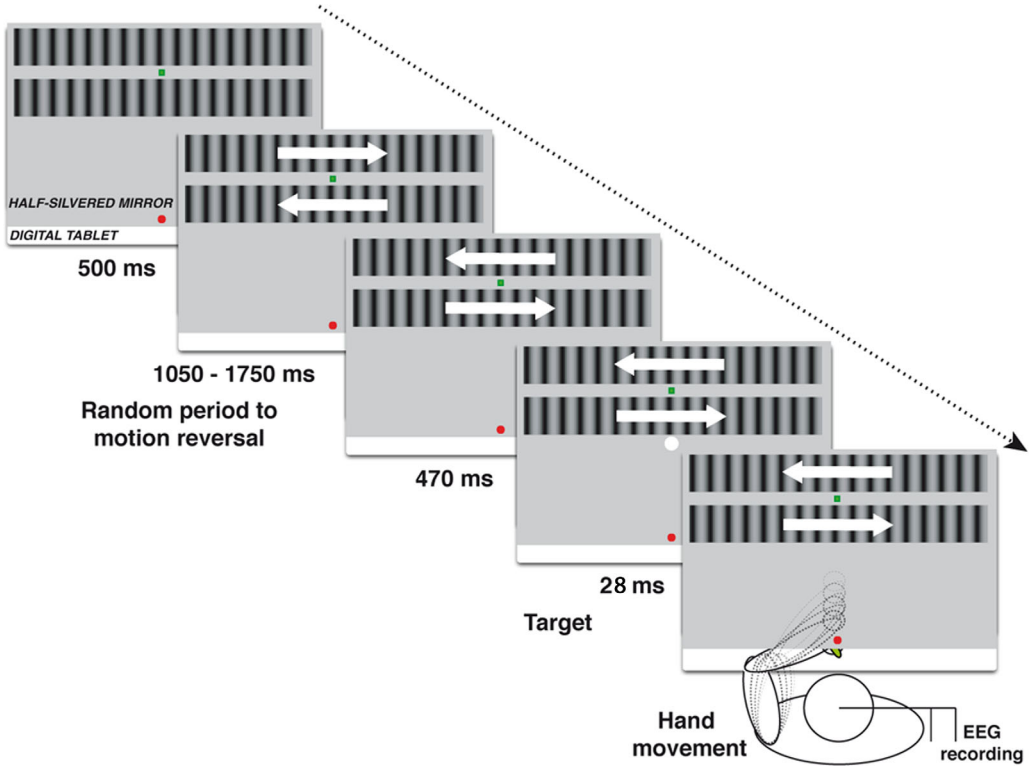


**Figure 1.** Task design and experimental setup. Schematic illustration of a standard 470 ISA trial. White arrows indicate the direction of motion. Participants fixated on a green square between the two gratings. The initial position of the hand was depicted with a red dot. We measured the hand's end point deviation at each ISA and compared it to an identical condition but with a static pattern. When the grating (the number of cycles do not necessarily match the actual used stimuli) was initially moving to the right, the influence of the motion signals was calculated by subtracting averaged hand end point position for initially rightward motion trials minus initially leftward motion trials, and vice versa (Whitney, Westwood, & Goodale, 2003). Vision was binocular, and the room was completely dark. Vision of the hand was occluded to ensure that the influence of motion on reaching was not due to visual information of the hand, and to exclude any effect of motion other than that caused by the stimulus.

& Horton, 2004; Standage & Benevento, 1983), carrying visual signals to V1 and MT in parallel (ffytche, Guy, & Zeki, 1995). In fact, both motion discrimination (Barbur, Watson, Frackowiak, & Zeki, 1993) and accurate pointing (Perenin & Jeannerod, 1975) persisted in patients with V1 lesions, reflecting the importance of nonprimary visual pathways in perception and action processing streams. Consequently, fast motion's influence on reaching (Gomi, Abekawa, & Nishida, 2006; Saijo, Murakami, Nishida, & Gomi, 2005) may not hinge on feedback connections to V1, but through MT affecting spatial codes at shorter latencies (Whitney et al., 2007).

To test this, we determined the motion-induced shift by quantifying the hand's end point deviation when reaching a stationary flash in the presence of motion. Visual evoked potentials (VEPs) were used as a measure of electrophysiological activity in the visual cortex. We found that motion delayed the detection of the flash, and that this delay determined the size of the hand shift, suggesting a predictive strategy to extend the beneficial use of motion through feedforward circuits. Finally, we observed an early pattern of extrastriatial activity as a causal contributor to the slowed sensory response.

## Method

### Participants

Twenty right-handed naïve volunteers (10 women; $M = 23.6$, $SD = 2.6$ years) participated in the experiment. Uncorrected deficits in visual acuity or neuromuscular disorders were not reported. Prior to the experiment, participants provided written informed consent. The study was approved by the local ethics committee in accordance with the Declaration of Helsinki.

### Apparatus and Behavioral Data Acquisition

Participants sat in front of a digital tablet (Calcomp DrawingBoard III 34240), which was (vertical distance) 48–50 cm below the eyes. Virtual stimuli were generated by an Apple MacPro 2.6 GHz Quad-Core and displayed by a Mitsubishi SD220U projector (72 Hz, 800 × 600 pixels). The stimuli were viewed through a half-silvered mirror between the projected image and the digital tablet, in order to perceive the image on the tablet where the movements were executed (Figure 1). Participants used a stylus (which we will refer to as the hand position) to perform the task underneath the half-silvered mirror. Its position on the tablet was recorded at 200 Hz with a 0.01-mm spatial resolution.

### Stimulus Design and Procedure

Two sinusoidal gratings with a contrast of 100% moved horizontally in opposite directions (speed 12.8°/s, time frequency of 10 Hz, and spatial frequency of 0.78 cycles/degree), each subtending 5.7° × 26.7° on a dark background (0.02 cd/m$^2$; Whitney, Westwood, & Goodale, 2003). This speed of motion, lower than 16°/s, allowed the visual system to similarly integrate local luminance of

stationary and moving objects (Burr, 1981). Participants fixated their gaze on a green square located between the gratings. In each trial, the position of the fixation point varied laterally within a range of 3 cm (∼3.43°). The gratings remained static during the first 500 ms and then began to drift for a period between 1,050 and 1,750 ms. After this time, the gratings reversed their direction and continued moving for an equivalent period of time. The initial direction of the gratings was randomized in each trial. An additional condition with a static grating was added to the experiment as a control condition. Either before or after the motion reversal, a target flash (80.5 cd/m$^2$) consisting of a disk of 2 cm in diameter was presented for two frames (∼27.8 ms). The target was randomly presented at five different times (interstimulus asynchrony [ISA] from −720 ms before to 470 ms after the motion reversal: −720, −235, 0, 275, or 470 ms), as presented in previous studies (Whitney, Westwood, & Goodale, 2003). By combining stimulus onset before, at, and after the motion reversal, these different ISA allowed us to test the influence of motion on the hand reaching across time, and to detect the reversed effect when motion changed to the opposite direction. In the static condition, the fixed timing of the flash onset was identical to the moving condition, even though there was no motion reversal. The lateral ($x$) coordinate of the target location varied randomly from trial to trial (−3, 0, or 3 cm), to prevent subjects from using stereotyped movements to memorized positions. The sagittal ($y$) location of the target remained always constant ($y = 20$), 3 cm below the nearest grating. The starting position was at the origin of coordinates. The distance between the starting position and the target was thus approximately 20 cm.

Participants were instructed to perform a fast movement to reach the target's position as accurately as possible. We encouraged participants to refrain from making excessive body and head movements, although they were not physically restrained to prevent the subject's behavior from being different than in natural conditions (Steinman, Kowler, & Collewijn, 1990). A velocity threshold of 50 mm/s was used to detect the beginning and the end of the hand movement (Neggers & Bekkering, 2002; van Beers, Haggard, & Wolpert, 2004). Each participant completed 27 blocks (18 moving, 9 static) of 100 trials distributed on 2 different days. One minute of rest was given between each block. Half of the blocks were performed with the right hand and the other half with the left hand, ensuring the control of possible motor asymmetries in the EEG data. Consequently, there were 90 trials for each hand, motion, and ISA. All conditions were counterbalanced across participants.

### Behavioral Analysis

Data recording began 200 ms before the onset of the stimulus and ended 500 ms after the end of the movement. We registered the $x$ (lateral) and $y$ (depth) tablet coordinates of the hand trajectory for each trial. The relevant error (i.e., motion-induced hand shift) was that observed along the lateral dimension, defined as the distance between the target and the hand end point position in the abscissa axis. A negative pointing bias indicated that the hand movement ended at the left of the target, and vice versa. The motion-induced mislocalization was determined by the absolute value of subtracting the bias in the static condition from the bias in the moving condition. We conducted a 2 × 5 repeated measures analysis of variance (ANOVA) with factors motion (static, moving) and ISA (−720, −235, 0, 275, 470 ms) to determine their influence on the hand end point position. Left and right hand movements were collapsed since preliminary analysis of handedness effect, Handedness × Motion, and Handedness × ISA interactions did not yield any statistically significant effect ($p > .18$ for all comparisons). The ISA with the larger motion-induced hand shift was considered as high mislocalization, whereas the ISA with the minimum motion-induced hand shift was defined as low mislocalization. We further tested whether differences between the two (moving vs. static) average values of hand end point position were similar through ISAs, using post hoc paired $t$ tests corrected for multiple comparisons. Trials where reaction times were out of the 200–800 ms range were discarded from the analysis.

### EEG Acquisition and Analysis

Continuous EEG signal was acquired to register early VEPs for all experimental conditions. EEG was recorded from the standard 32-electrode arrangement mounted in an elastic cap (Electro-Cap) referenced online against the right mastoid electrode and rereferenced offline against the half mean of the left mastoid. The electrodes were located at standard 10/20 positions: F3/4, C3/4, P3/4, O1/2, F7/8, T3/4, T5/6, FC1/2, FC5/6, CP1/2, CP5/6, PO1/2, Fz, Cz, Pz. Frontopolar electrodes together with frontocentral and occipital midline sites were not used, leaving a total of 27 electrodes. We monitored eye movements with electrodes placed above and below the right eye, and on the outer canthi of the left and right eyes, respectively. Electrode impedances were kept below 5 kΩ. The electrophysiological signals were sampled at 250 Hz and filtered online with a band-pass of 0.01–50 Hz (half-amplitude cutoffs). Trials with base-to-peak electrooculogram (EOG) amplitude of more than 50 $\mu$V, amplifier saturation or a baseline shift exceeding 200 $\mu$V/s were automatically rejected (Cunillera, Gomila, & Rodriguez-Fornells, 2008). As a result, although online eye tracking was not assessed in order to reproduce Whitney's paradigm as accurately as possible, eye movements were constantly monitored to separate blink and blink-free trials for the subsequent ERP analysis.

Stimulus-locked ERPs for artifact-free trials were averaged over epochs of 400 ms, including a 100-ms prestimulus baseline. Only participants with at least 75 artifact-free trials for each response hand, motion direction, and ISA were included in the analysis ($N = 18$). After averaging, epochs were low-pass filtered with a cutoff frequency of 30 Hz in order to facilitate the peak's measurement of the VEPs (Rodionov, Goodman, Fisher, Rosenstein, & Sohmer, 2002). We specifically measured the peak latency of the visual N1 component, the primary VEP elicited by the perception of the flashed object. The peak of the N1 was defined as the most negative value within the 0–270 ms time window (Cunillera et al., 2008). We submitted N1 latency values to an ANOVA that included two within-subjects factors: motion (static, moving) and electrode (19 levels: Fz, T3, CP5, C3, CP1, Cz, CP2, C4, CP6, T4, T5, P3, Pz, P4, T6, PO1, PO2, O1, O2). The hand (left or right) was not considered as a factor, since preliminary analyses revealed a lack of statistical main effects and interactions ($p > .31$ for all comparisons). For an easier visualization, we therefore collapsed hand factor with the right-left flip of the hemispheres in trials performed with the left hand to align ipsilateral and contralateral channels (Stevens, Calhoun, & Kiehl, 2005). Motion × Electrode interaction was decomposed by selecting 12 of these 19 electrodes for a topographical analysis according to three factors (Cunillera, Toro, Sebastian-Galles, & Rodriguez-Fornells, 2006): hemisphere [two levels: contralateral (T3, T5, O1, C3, P3, PO1), ipsilateral (T4, T6, O2, C4, P4, PO2)]; laterality [two levels: lateral (T3, T5, O1, T4, T6, O2), central (C3, P3, PO1, C4, P4, PO2)]; and anterior-posterior [three levels: anterior (T3, C3, T4, C4), medial

(T5, P3, T6, P4), posterior (O1, PO1, O2, PO2)]. This analysis was carried out on data corrected using the vector normalization procedure (McCarthy & Wood, 1985).

We then investigated N1 latency in static and moving conditions as a function of the ISA, confined to the region that showed a maximum effect (parietocentral region, Pz electrode). Post hoc analyses using paired $t$ tests were performed when appropriate. Finally, we conducted Pearson bivariate correlations to test the relationship between the behavioral outcome and the electrophysiological data using a linear regression analysis. Two ISA values were not considered: First, −235 ISA was discarded since hand position was affected by online corrections during reaching, distorting the motion-induced hand shift (Whitney, Westwood, & Goodale, 2003). Second, preliminary analysis of 275 ISA showed that motion-reversal VEPs modulated both the N1 amplitude and latency, making the data not suitable for linear regression analysis (Kuba, Toyonaga, & Kubova, 1992).

### Current Source Density Analysis

Current source density (CSD) is a reference-free technique that computes the second spatial derivative (Laplacian) of the scalp electric potential. Laplacian provides the location, direction—entering (*sinks*) or leaving (*sources*) the scalp (Nunez, 2006)—and intensity of the radial current flow that determines an ERP topography (Mitzdorf, 1985; Perrin, Pernier, Bertrand, & Echallier, 1989). Using CSD, we aimed to track down the possible neural substrate of the motion-induced hand shift. CSD estimates permitted us to refine the voltage source localizations of the earliest VEPs at the initial stages that succeed the target onset. We therefore transformed all of the averaged ERP waveforms into reference-free CSD estimates ($\mu V/cm^2$ units, head radius = 10 cm). We used the spherical spline surface Laplacian (Perrin et al., 1989) with standard computation parameters (50 iterations; spline flexibility $m = 4$; smoothing constant $\lambda = 10^{-5}$) previously established for our 27-channel recording montage. Similar arrangement of electrodes in magnetoencephalography/EEG studies has been used in previous CSD analysis to search the current generator of early VEPs (Bartsch et al., 2014) and P300 ERP component (Klein, Andresen, Berg, Kruger, & Rockstroh, 1998).

As ERP data, separate stimulus-locked CSD waveforms for artifact-free trials were averaged over epochs of −100 ms to 400 ms for each condition. Nonetheless, we examined CSD estimates of the first 0–100 ms to determine the earliest differential activity between moving and static conditions that may explain the N1 morphology. CSD estimates for high and low motion-induced hand shift at temporal, occipital, and parieto-occipital electrodes were submitted to a repeated measures ANOVA that included four within-subjects factors: mislocalization (high, low), motion (static, moving), electrode (T5, T6, PO1, PO2, O1, O2), and time (0–20, 20–40, 40–60, 60–80, 80–100 ms). Hand factor was collapsed given its lack of main effect and interactions ($p > .4$ for all comparisons), and hemispheres were swapped. Preliminary analyses of CSD estimates discarded the hemisphere (contralateral or ipsilateral) as a relevant factor, since they revealed a lack of statistical main effect and interactions ($p > .2$ for all comparisons). We systematically assessed the source of interactions by calculating pairwise comparisons using paired $t$ tests. $T$ tests were also applied specifically to the peak of the sink/source component (48–72 ms). Finally, we conducted Pearson correlations to analyze the relationship between the N1 latency and the amplitude of the early CSD estimates. Time windows for the measurement of early CSD mean amplitudes were defined on the basis of the peak of the sink/source activity (60 ms) within a ± 12-ms time window (48–72 ms). Both in ERP and CSD analysis, Bonferroni's and Greenhouse-Geisser epsilon correction were applied (Jennings & Wood, 1976).

### Source Localization Analysis

Brain Electric Source Analysis (BESA 2000 version 5.3; Scherg, 1990) was used to model the anatomical sources of the neural correlates underlying motion-induced shifts in reaching. To that end, we used the difference waveform obtained subtracting static minus motion in the high mislocalization (ISA = 0 ms). BESA algorithm consists of an inverse method that computes the location, orientation, and sequence of activation of multiple equivalent dipolar sources by calculating the voltage scalp distribution that would be produced by a given source activation and comparing it with the original scalp distribution. Following previous descriptions of the neural sources of early VEPs (Clark, Fan, & Hillyard, 1994), modeling was performed across a window of 60 ms around the VEP peak (i.e., 40–100 ms). We used the standard BESA four-shell spherical head model with relative conductiveness of 0.33, 0.33, 0.0042, and 1 for the head, scalp, bone, and cerebrospinal fluid, respectively, and sizes of 85 mm (radius), 6 mm (thickness), 7 mm (thickness), and 1 mm (thickness). We fitted one single dipole to the N1 onset based on its occipital topography, and two symmetrical dipoles were subsequently fitted near the bilateral temporo-occipital regions. The latencies of major peaks in the dipole source waveforms were taken as indices of neural response timing. The dipole pair was constrained to be mirror image in location only. Interactive changes varying source location and orientation led to minimization of the residual variance between the model and the observed spatiotemporal VEP distribution (Scherg 1990). The resulting source configuration presents the best model fit for the given number of sources in the whole time epoch analyzed (nonlinear least squares fit; Schneider, 1972). The final location of each dipole was projected using the BESA standard MRI, which assumes a realistic approximation of the head based on the MRI of 24 individuals in Talairach space (Talairach & Tournoux, 1988), with a voxel grid of 6 mm and a regularization parameter singular value decomposition (SVD) per cent of 0.001.

### Granger Causality Analysis

We employed Granger causality analysis (GCA) to estimate the directionality of the neural interactions underlying the pattern of the scalp potential. GCA has become a useful tool to statistically predict the amount of variance in signal X that can be determined by the past of signal Y and X, better than relying on the past of signal X alone (Granger, 1969). Granger causality is implemented by multivariate autoregressive (MVAR) modeling, in which a set of time series is modeled as weighted sums of past values. We adopted the Granger Causal Connectivity Analysis (GCCA) toolbox (Seth, 2010), widely accredited in electrophysiological studies (Hesse, Moller, Arnold, & Schack, 2003; Zhang & Ding, 2010).

Both unfiltered time-domain CSD and source signal were used to estimate the direction of the synaptic transmission between the early VEPs elicited in the temporo-occipital region and the representative area where the delay of the visual N1 was sharply observed (Pz). In particular, the two time series pooled for the analysis were: (1) T5, O1, and PO1 electrodes at 60 ms, and (2) Pz electrode at 200 ms (peak of the visual N1), both within a ± 50-ms time window to ensure sufficient number of observations

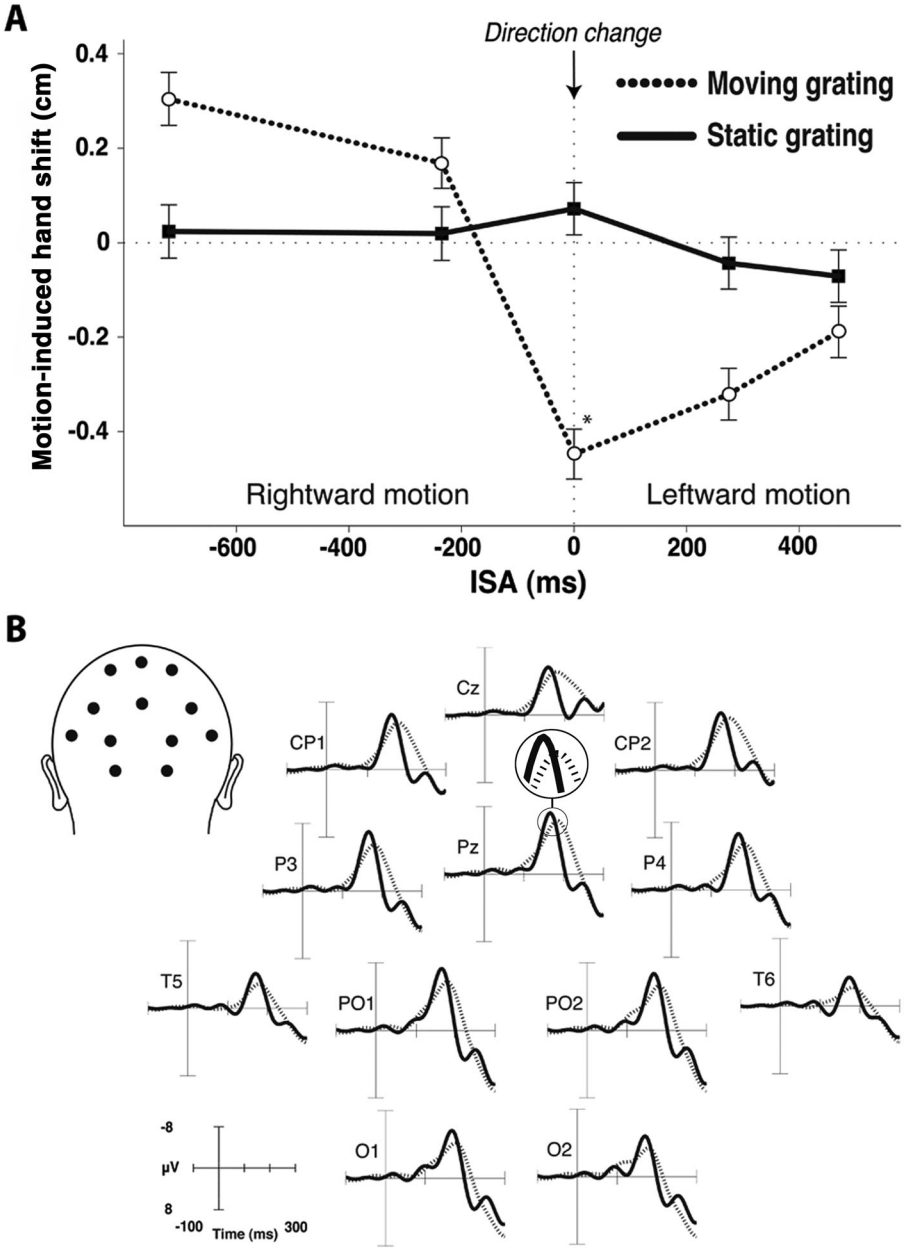


**Figure 2.** Behavioral (A) and electrophysiological (B) effects after adaptation to visual motion averaged for all ISAs. A: Motion-induced hand shift for each ISA. Data have been merged so that the nearest horizontal grating to the target was initially rightward (inverse pattern when initial direction was leftward). The motion reversal is depicted by the vertical dotted line at 0 *x* axis. Positive values of motion-induced hand shift thus reflected that the hand ended at the right of the target, and vice versa. Error bars show *SEM* $*p < .05$. B: Grand-average ($N = 18$) stimulus-locked ERP waveforms from 12 representative scalp locations in response to the corresponding static (solid line) and moving (dotted line) patterns displayed in panel A (averaged across ISAs). [Correction added on 8 September 2015, after first online publication: Legend for Figure 2A indicating motion reversal has been amended.]

(Seth, 2010). These selections were based on the optimal surrounding of the VEPs of interest and to avoid a predominantly unidirectional driving from one channel to the other (Wang, Chen, & Ding, 2008). Ipsilateral hemisphere was not added to the GCA in the CSD space since none of the temporo-occipital electrodes (T6, O2, PO2) reached statistical significance in the previous analysis. For each participant, we preprocessed data from targeted electrodes by calculating and subtracting the ensemble mean from each single trial, providing a zero-mean status required for MVAR model fitting. All mean-corrected data were checked for covariance stationarity (i.e., the mean and variance of each time series do not change over time). We used the KPSS test (Kwiatkowski, Phillips, Schmidt, & Shin, 1992), and the null hypothesis $H_0$ of no stationarity was rejected at a 5% confidence level ($p$ values $> .15$ for all time series).

We defined the optimal number of past observations to incorporate in the regression model with the Akaike information (Akaike, 1974), setting the VAR model order at 10 for CSD data and at 9 for source signal. We applied conditional G causality for preprocessed data, and Granger $F$ tests were conducted on model residuals to

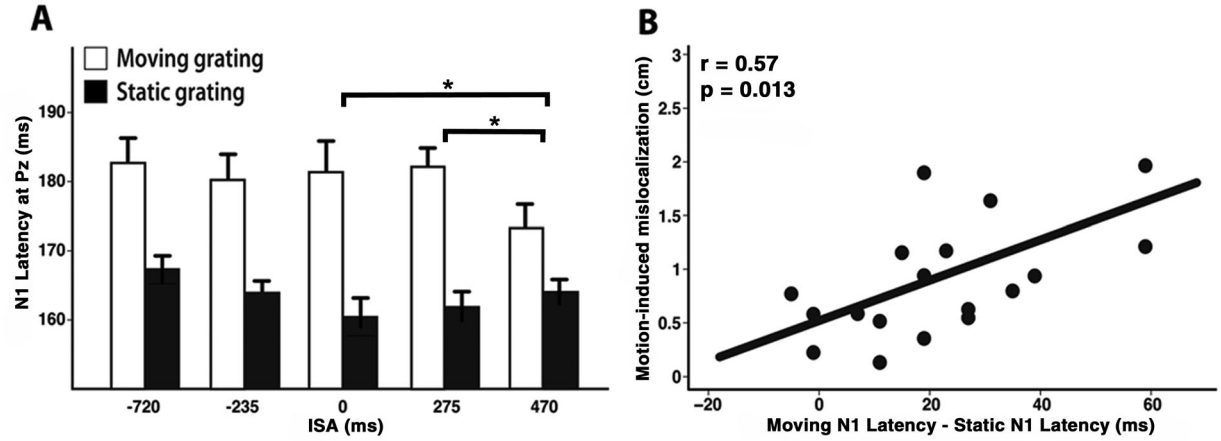


**Figure 3.** Peak latency of N1 VEP. A: N1 latency ($M \pm SEM$, $N = 18$) at Pz electrode in the presence (white) and absence (black) of visual motion for each of the five ISAs. *$p < .05$. B: Correlation between the motion-induced mislocalization and the difference in N1 peak-latency when subtracting static from moving condition at 0 ISA.

probe a putative causal influence of electrode/dipole Y in electrode/dipole X. Statistically significant sets of G causality interactions were defined below a $p$ value of .01 and after correction for multiple comparisons. The strength of the MVAR model was determined by a model consistency higher than 80% (Seth, 2010). Static condition did not show a source/sink temporo-occipital activity at 60 ms, and its model consistency was consequently under 80% (66.1%), being discarded from the G causality analysis.

Time-variant GCA (Hesse et al., 2003) was applied to significant causal interactions in order to detect when the maximum values of G causality peaked. Time-domain causal flow of each electrode was inferred from significant G causalities. The causal flow of a given node in a causal network (weighted or unweighted by the number of nodes) is defined as the difference between its ingoing and outgoing connections.

## Results

### Behavioral Results

Hand end point position was different across ISAs, $F(4,68) = 10.44$, $p < .001$, $\varepsilon = .66$ (see Figure 2A) and, more importantly, the end point position at each ISA was modulated by the absence or presence of visual motion (Motion × ISA: $F(4,68) = 17.11$, $p < .001$, $\varepsilon = .64$). At comparable eccentricity and motion speed, the magnitude of the effect in terms of degrees of the visual angle was 8.83°, roughly similar to previous studies with vertical background motion (Whitney, Westwood, & Goodale, 2003). Quantitatively, highest and lowest motion-induced hand shift were found at ISA = 0 ms and ISA = 470 ms, respectively. Further pairwise comparisons between moving and static conditions at each ISA confirmed that the motion-induced shift of the hand was significantly higher only when the target was presented at the same exact moment of the motion reversal (0 ISA; $t(17) = -3.08$, $p = .02$ corrected). The rest of the moving versus static comparisons were not significant ($p > .07$ for all comparisons).

### ERP Results

We compared static and moving grand-average ERP waves from −100 ms prestimulus to 300 ms poststimulus of the occipital, temporal, parietal, and centroparietal electrodes (Figure 2B). Latency values of the visual N1 component were longer in the presence of visual motion, $F(1,17) = 51.32$, $p < .001$. The topographical analysis showed a significant effect of electrode, $F(18,306) = 2.71$, $p = .037$, and Motion × Electrode interaction, $F(18,306) = 2.64$, $p = .029$, indicating differences in the topographical distribution of the motion main effect. Decomposition of the interaction revealed that the slower sensory processing in the presence of visual motion had a parietocentral (Pz) maximum (Motion × Laterality, $F(1,17) = 10.72$, $p = .004$). No significant effects were found either in Motion × Hemisphere, $F(1,17) = 0.23$, $p = .63$, or in Motion × Anterior-Posterior, $F(1,17) = 0.34$, $p = .71$, interactions.

We subsequently examined how the N1 peak latency at Pz varied as a function of the ISA (Figure 3A). The analysis revealed a marginal main effect of ISA factor, $F(4,68) = 2.41$, $p = .058$. More importantly, the delayed N1 latency in the moving condition was not exclusively enhanced by the exposure to visual motion, but was different across ISAs, $F(4,68) = 2.71$, $p = .03$. Pairwise comparisons showed that the lag of N1 latency at 0 ISA, $t(17) = 3.13$, $p = .025$, and at 275 ISA, $t(17) = 3.04$, $p = .03$, was significantly longer than that at 470 ISA. The fact that the lags at 0 and 275 ISA were not statistically different ($p = .61$) discards the possibility that the behavior–N1 correlation at 0 ISA might be due to attentional-attraction effects of the motion reversal. Otherwise, the simultaneity of the target onset and the motion reversal at 0 ISA would reflect higher lags of the N1 latency in the presence of visual motion, but 275 ISA showed practically the same effect. The rest of comparisons were not significant ($p > .19$). These results thus point to different latency delays depending on the size of the motion-induced hand shift, suggesting that motion effect in position coding affected the N1 morphology by inducing a slower sensory processing.

We further correlated the behavioral differences observed between static and moving conditions with their electrophysiological outcome. Pearson correlations between the size of the motion-induced mislocalization (absolute value of subtracting motion-induced hand shift of moving from static condition) and the difference in the N1 peak latency were performed at each ISA. Two values were excluded (see Method). Participants with higher motion-induced hand shift presented longer temporal shifts of the N1 latencies at 0 ISA, $r(16) = .57$, $p = .013$ (see Figure 3B). Noteworthy, previous pairwise comparisons showed that the 0 ISA condition yielded the strongest effect on both the motion-induced hand

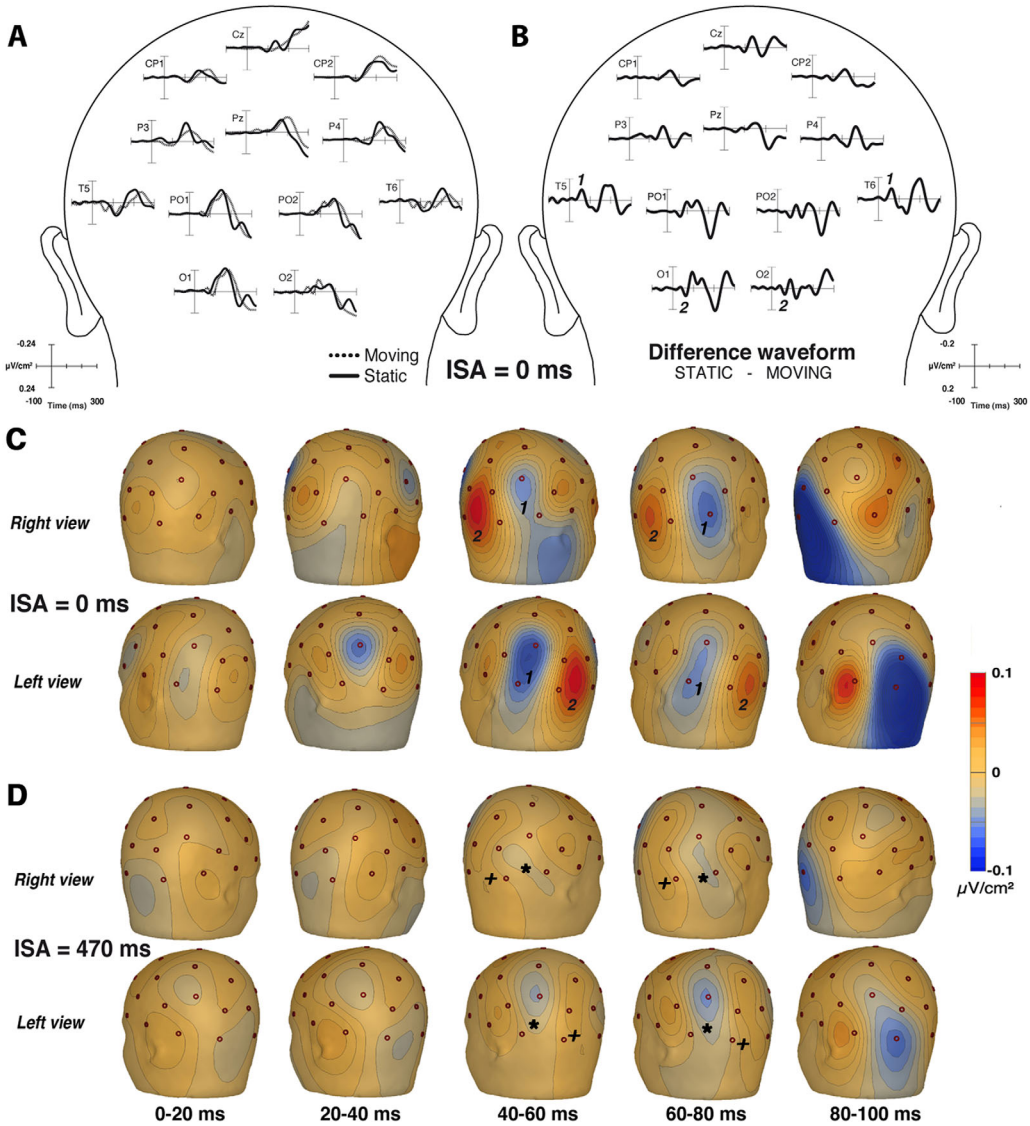


**Figure 4.** CSD waveforms. A: Grand-average ($N = 18$) stimulus-locked CSD waveforms at 0 ISA for each motion condition and their respective difference waveform (static minus moving, B). C: 3D isovoltage topographical mapping illustrating the scalp distribution of the CSD difference waveform from 0 to 100 ms for each hemispheric view. Post hoc comparisons between moving and static CSD estimates reported higher activity with the presence of visual motion at 40–60 ms (T5: $t(17) = 13.12$, $p < .001$; O1: $t(17) = 2.36$, $p = .03$; PO1: $t(17) = 2.14$, $p = .047$; O2: $t(17) = 2.18$, $p = .043$), at 60–80 ms (negativity in T5: $t(17) = 3.27$, $p = .005$; and T6: $t(17) = 6.87$, $p < .001$) and at 80–100 ms (positivity in O1: $t(17) = 7.28$, $p < .001$; PO1: $t(17) = 3.88$, $p = .001$; and O2: $t(17) = 2.87$, $p = .009$). In contrast, 470 ISA (D) only showed higher activity at 60–80 ms in T6, $t(17) = 2.84$, $p = .01$, and at 80–100 ms (O1: $t(17) = 3.81$, $p = .001$; PO1: $t(17) = 2.85$, $p = .01$). Note the lack of differential morphology, in 470 ISA, at temporo-occipital (negativity [*] in T5, T6), parieto-occipital (PO1, PO2), and occipital (positivity [+] in O1, O2) scalp locations around 60 ms after the target onset. We also compared moving and static CSD estimates at specifically $60 \pm 12$ (48–72 ms): 0 ISA (high mislocalization) unfolded significant higher neural activity in all electrodes when visual motion was present (T5: $t(17) = 15.72$, $p < .001$; T6: $t(17) = 11.61$, $p < .001$; O1: $t(17) = 3.41$, $p = .004$; O2: $t(17) = 3.37$, $p = .036$; PO1: $t(17) = 2.98$, $p = .008$; PO2: $t(17) = 3.11$, $p = .006$), whereas in 470 ISA condition, only T6, $t(17) = 3.23$, $p = .005$, and PO2, $t(17) = 2.21$, $p = .04$, were significant.

shift and the delay of N1 peak. The rest of ISAs showed weaker or nonsignificant correlations, in consonance with the reduction of the motion effect (−720 ISA, $p = .26$; 470 ISA, $p = .76$). Apparently, the strength of the correlation tended to decrease when both behavioral and electrophysiological differences diminished.

### CSD Estimates

CSD analysis evaluated the topographical distribution of current sources and sinks on the scalp. We found that motion signals induced a different morphology of the early modulations at temporo-occipital sides between 40 and 80 ms after the target onset (Figure 4C for 0 ISA; Figure 4D for 470 ISA).

A significant four-way interaction (Mislocalization × Motion × Time × Electrode; $F(20,340) = 2.64$, $p < .001$) revealed that differences between moving and static CSD estimates in each electrode through time were modulated depending on the size of the motion-induced hand shift. At 0 ISA (high mislocalization), motion elicited a positive current flow in temporal areas of both hemispheres (T5/T6) around 60 ms after the target onset (Figure 4A,

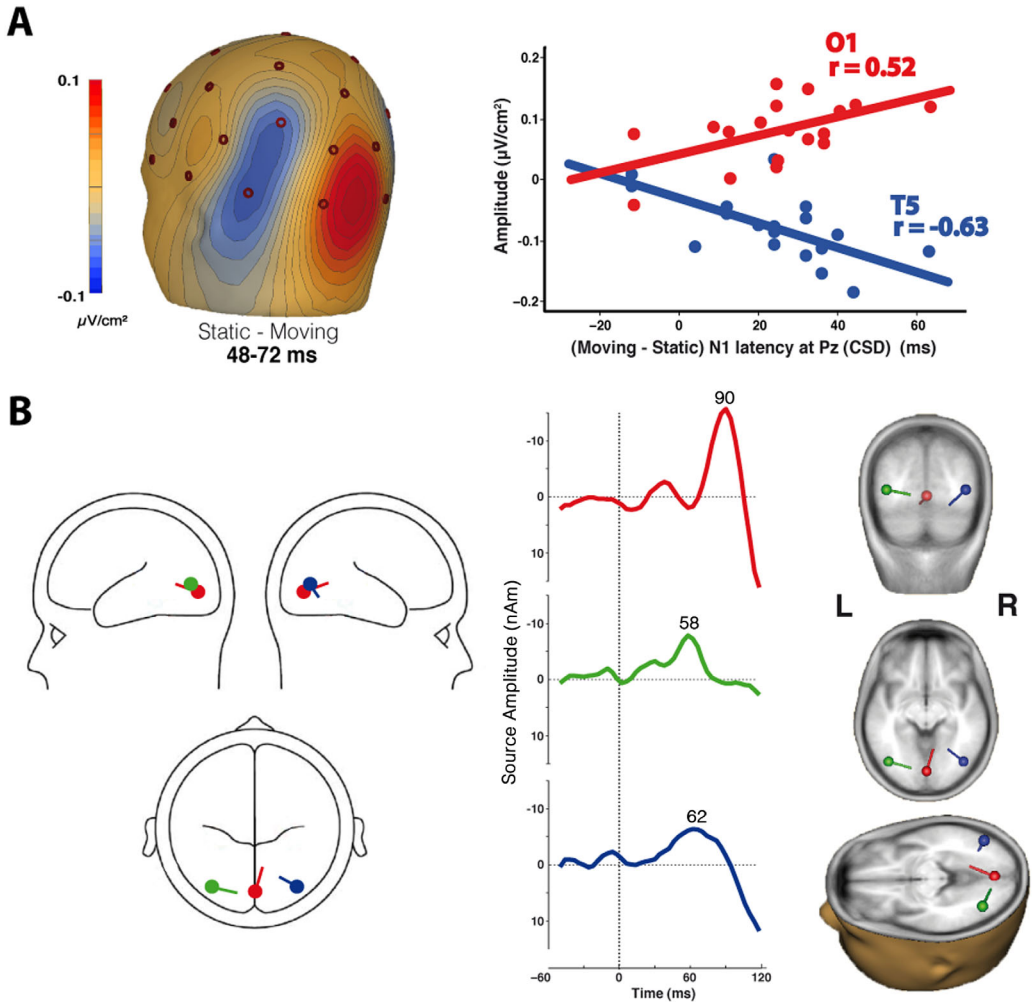


**Figure 5.** Source/sink correlations and the correspondent source localization analysis at 0 ISA. A: Pearson correlations between the CSD estimates of the difference waveform at the temporo-occipital scalp locations (T5 in blue, O1 in red) and the delay of the visual N1 peak at the parietocentral region (Pz). For each participant, the scatter plot depicts the delay in the N1 peak latency as a function of the mean amplitude at the source/sink locations. B: Dipole model for the neural sources of the (static minus moving) ERP difference waveform. Both dipole 1 (red; $x = -0.1$, $y = -78.9$, $z = -3.0$, Talairach space) and symmetric dipoles 2 (green) and 3 (blue) ($x = \pm 37.4$, $y = -70.4$, $z = 4.9$, Talairach space) were fit over the 40–100 ms interval. Time course of each computed dipole is represented in the source waveform. Images on the right show the anatomical location of each dipole.

dotted line). Also, occipital (O1, O2) and partially parieto-occipital (PO1, PO2) regions exhibited a concurrent negative peak. In the corresponding difference waveform (Figure 4B), we observed a negative component in T5 site at 40–60 ms, which shows inverted polarity at parieto-occipital electrodes (PO1 or O1). The scalp distribution of this CSD component reflects a temporo-occipital source/sink activity from 40 ms to 80 ms (Figure 4C), being more active when participants committed a higher motion-induced hand shift reaching the object. Noteworthy, CSD components of the difference waveform when subtracting static from moving conditions were mainly originated by differential activity elicited in the moving condition, whereas static CSD estimates remained closer to zero.

We subsequently correlated the mean CSD amplitude of the difference waveform with the lag of the N1 CSD estimates, to test whether the source/sink activity interacted not only with the behavioral outcome but also with the speed of sensory processing. The shift in N1 latency highly correlated with T5, $r(16) = -.63$, $p = .005$ (see Figure 5A) and O1, $r(16) = .52$, $p = .02$, amplitude, but not with PO1 ($p = .44$). The ipsilateral hemisphere yielded marginal correlation in all electrodes: T6: $r(16) = -.44$, $p = .07$; O2: $r(16) = .44$, $p = .06$; and PO2: $r(16) = .43$, $p = .07$ [Correction added on 8 September 2015, after first online publication: values of $r(16)$ for T5 and T6 have been amended.]. These results indicate that participants with longer N1 delays also presented higher temporo-occipital activation 60 ms after the target onset.

### Source Localization

The neural sources of early VEPs at 0 ISA were explained by a three-source model with one single dipole located in V1 and two symmetrical sources situated in the left/right extrastriate cortex (Figure 5B, Talairach coordinates in figure caption). This three-source model accounted for up to 90% of the variance in the scalp distribution over the 40–100 ms time window, with a residual variance of 9.3%. Source waveforms of symmetric dipoles showed nearly identical peak latency at approximately 60 ms, whereas the time course of V1 source had a later peak at 90 ms. These data

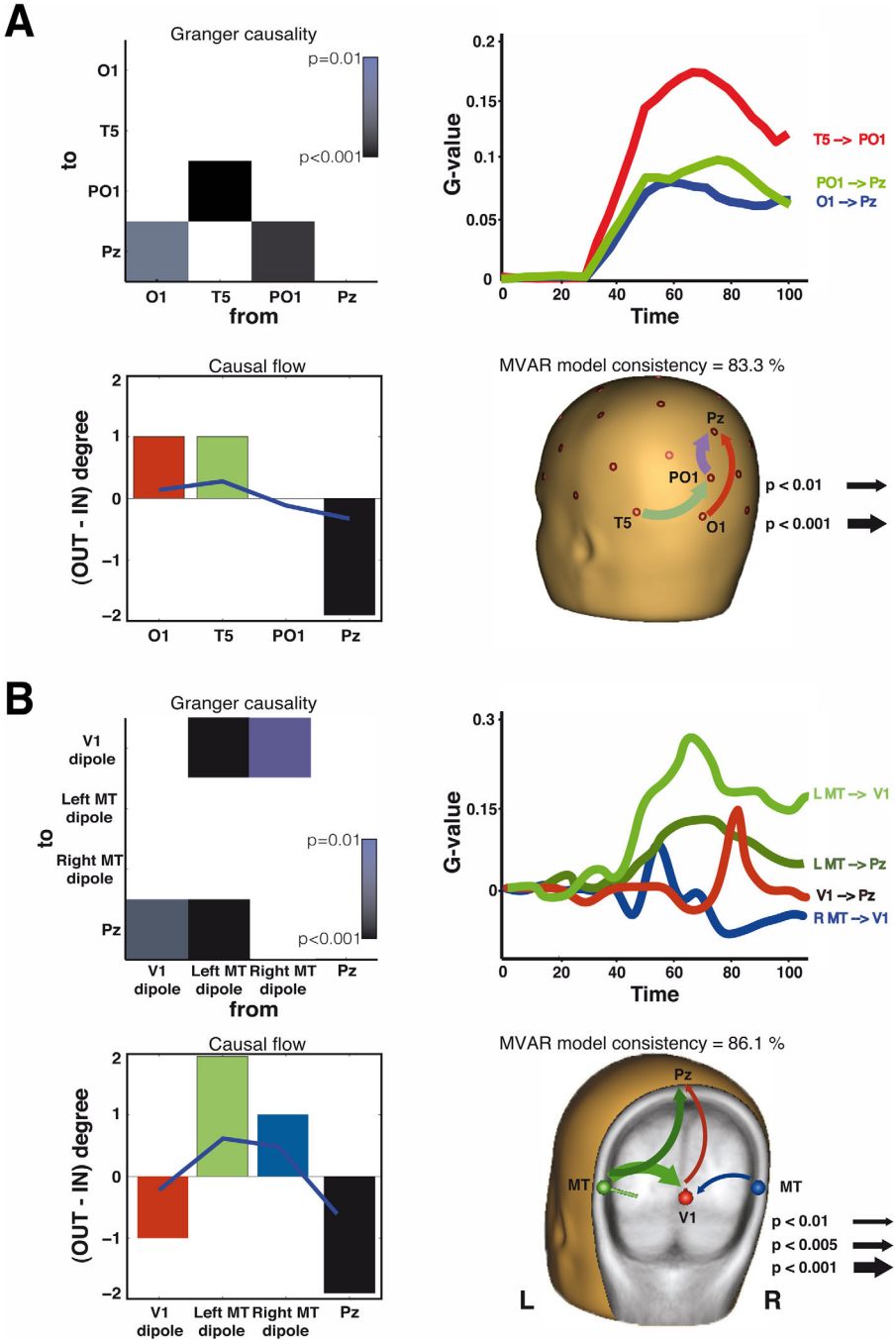


**Figure 6.** GCA at 0 ISA moving condition for the contralateral hemisphere in CSD (A) and source (B) signal. Upper left: G causality significant ($p < .01$) network interactions between each node, representing the level of significance as a function of color darkness. Upper right: G values of significant interactions across time. Lower left: bar plot with unweighted (bars) and weighted (lines) net Granger causal flow for each scalp location. Positive values of causal flow corresponded to causal source regions with higher outgoing causal connections, whereas negative causal flow represented inflow hubs. PO1 electrode, for example, has one causal flow input and one causal flow output, which results in a 0 (OUT-IN) unweighted degree. Lower right: network of significant causal connectivity with a dominant directional influence.

support the hypothesis that a fast V1-independent mechanism through nonprimary visual pathways might be the first to convey the influence of motion in position coding.

### Granger Causality Estimates

The results extracted from the GCA in the CSD space denoted significant direct causal influence from O1 → Pz ($p = .006$; Figure 6A, upper left panel) and from PO1 → Pz ($p < .001$). At the same time, T5 → PO1 was also significant ($p < .001$), suggesting an indirect causal interaction from T5 to Pz. Model consistency (i.e., part of the data that fitted the model) was higher than 80% (83.31%). Granger causality estimates of each significant interaction were also analyzed as a function of time (Figure 6A, upper right panel). We observed that maximum instantaneous G values peaked between 60 and 70 ms—around 80 ms in the PO1 → Pz

interaction—suggesting that their highest contributions to the Pz signal coincided with the peak latency of the temporo-occipital CSD component. The analysis of the causal flow (Figure 6A, lower left panel) shed light on the configuration of the causal network underlying the dominant CSD topographies. Noteworthy, the network revealed T5 and O1 locations as sources nodes with a significant outflow towards parietal areas (Figure 6A, lower right panel). In contrast, parietal lobe (Pz) had the highest number of incoming connections (causal sink). The GC analysis on source signal showed a similar profile with significant direct causal influence from the dipole in left MT to both Pz ($p < .001$) and V1 dipole ($p = .003$; Figure 6B). Additionally, V1 dipole also causally contributed to Pz profile ($p = .008$). On the right hemisphere, a weaker causal influence of MT dipole was found to influence V1 source ($p = .009$). Model consistency reached 86.12%. Based on the descriptive GCA results presented above, the parietocentral region—where the delay of the N1 was sharply observed—might act as an inflow hub of temporo-occipital connections during the period between 150 and 250 ms after target onset. Extrastriate activity at 60 ms would therefore be contributing crucially to the posterior N1 delay observed in higher motion-induced hand shift.

## Discussion

In the present study, we demonstrate that the motion-induced hand shift when reaching a stationary object correlates with a temporal delay of the visual N1, a primary VEP elicited by the perception of the object. Moreover, we provide evidence of early neural activity in the vicinity of the extrastriate cortex that causes the lag on N1 latency. These findings cast doubts on the feedback account as the putative neural mechanism that subserves the effects of motion in position coding. Instead, they imply a faster mechanism presumably channeled through nonprimary visual pathways. The speed of the sensory processing under the exposure to visual motion also reveals a predictive strategy invoked to maximize the use of motion signals in order to improve reaching accuracy, serving as a compensatory mechanism for neural delays when localizing objects in a dynamic scene.

Previous studies supported the effect of background motion signals on reaching, which induce hand end point shifts in the direction of the neighboring motion (Brenner & Smeets, 1997; Mohrmann-Lendla & Fleischer, 1991; Rodriguez-Herreros & Lopez-Moliner, 2008; Saijo et al., 2005; Whitney, Westwood, & Goodale, 2003). In agreement with this view, our results show that the hand position deviated either rightward or leftward consistent with the direction of the nearby motion. Our data also concur that the strongest effect of motion took place at the exact moment of the motion reversal (Whitney & Cavanagh, 2000), perhaps owing to an easier assimilation of the new motion direction following the change (Tse, Whitney, Anstis, & Cavanagh, 2011). However, the nature of this spatial offset is still debated, prompting a variety of potential explanations. It has been argued that position coding of a stationary object is processed differently than that of a moving object (Purushothaman, Patel, Bedell, & Ogmen, 1998), but the alternative idea of a common mechanism by which motion signals affect position's assignment of both stationary and moving objects has also gained validity (Durant & Johnston, 2004; Whitney & Cavanagh, 2000). A timing error was postulated to explain the spatial offset of motion-dependent phenomena with moving stimuli, such as the flash-lag effect (FLE; Murakami, 2001; Wojtach, Sung, Truong, & Purves, 2008). It is still to be determined, however, whether the cause of errors when estimating the location of a stationary flash could be related to temporal mechanisms. The correlation observed in the present study between the motion-induced hand shift and the delayed VEP latency points to a close link between spatial and timing errors. These results are in agreement with the idea that the speed of sensory processing of a flashed object is crucial when estimating its position, in such a way that the timing of the perception would determine the error in the pointing location (Durant & Johnston, 2004). Arguably, motion signals might delay the perceptual localization process of a stationary stimulus, by allowing extra time to use visual motion in order to update and recode the object's location. In our study, the temporal dynamics of the sensorimotor processing dovetail nicely with an anticipatory strategy also observed in FLE, based on longer neural latencies to flashed objects in comparison with responses to motion (Jancke, Erlhagen, Schoner, & Dinse, 2004). Additional time to process the perception of the flash might thus act as a compensatory strategy to improve visually guided behavior in dynamic environments. The observed time course is also consistent with oculomotor evidence of long-latency saccades showing a gradually built-up bias of saccade end points in the direction of motion (de'Sperati & Baud-Bovy, 2008). Indeed, perceptual delays related to saccades with longer latencies might depend on the recruitment of higher-order visual areas such as MT (Nishida & Johnston, 1999). Recent neurophysiological evidence supports this view, showing the crucial role of MT in the predictive coding framework (Vetter, Grosbras, & Muckli, 2013).

An extensive body of literature has validated MT as a key player in the discrimination and detection of visual motion. However, only recent neurophysiological evidence has shown that MT integrity is also critical when reaching stationary objects in the presence of nearby motion (Whitney et al., 2007). Our CSD and source localization analysis exhibited increased neural activity in the vicinity of MT when reaching was performed in the presence of motion. This activity was higher with the maximum motion-induced hand shift, which occurred when the object was presented at the exact moment of the motion reversal (Whitney & Cavanagh, 2000). In contrast, activity in the extrastriate cortex decreased for the lowest motion-induced hand shift. These findings lend credence to the hypothesis that motion processing might modulate the earliest stages of position coding (De Valois & De Valois, 1991), likely affecting the temporal coding of the perceived object location.

Anatomically, MT efferent backprojections to V1 were postulated as the neural pathways by which motion information altered position coding (Whitney & Cavanagh, 2000). According to this view, these feedback connections would continuously update the early representation of the target position hinging on motion information previously coded in MT (Whitney, Westwood, & Goodale, 2003). Thus, one possibility is that visual motion is processed more rapidly than the encoding of position. Psychophysical evidence reflects that motion's influence may act at various levels of the visual system (Fukiage, Whitney, & Murakami, 2011), with even nonhuman physiological findings revealing motion-induced position coding in the retina (Berry et al., 1999). In this regard, our data offer new electrophysiological insights about the timing of the early visual processes that assign stationary positions under the presence of visual motion. Source analysis demonstrates prior activity in the extrastriate cortex, peaking approximately at 60 ms, which is in line with electrophysiological studies that described very short latencies of visual responses in MT (Schmolesky et al., 1998), occasionally showing VEP components in MT before V1 (Buchner et al., 1997). Notably, CSD and source waveforms did

not show an earlier onset of the VEPs surrounding V1 previous to that observed in the extrastriate regions. In agreement with these results, GCA and CSD correlations strengthen the idea that this early neural activity at 60 ms affected the VEPs latency. First, the intensity of the preceding VEP component at extrastriate areas correlated with the longer N1 latency later detected. Using GCA, we also identified a causal influence of this activity in the lag of VEP peak latency, on both CSD and source signal. Specifically, we selected the VEPs of interest (i.e., VEP at 60 ms and N1 peak) by defining time windows that covered these elicited responses completely, being then nonsimultaneous. Our GCA approach is thus blind as to how changes in the time-window selection, either extending or shortening, and the lack of simultaneity could alter the resultant causal influence of the network. Overall, our findings suggest that the neural underpinnings by which motion exerts powerful influences on object manual localization may affect the initial phases of sensory processing (De Valois & De Valois, 1991), nearly parallel to the arrival of visual input to V1 (ffytche et al., 1995).

The hierarchical levels of the visual cortex have been shown to require around 100 ms to launch the cascade of feedforward connections from V1 and reach the higher-level areas, including MT (Nowak & Bullier, 1997). It is therefore conceivable that MT recurrent connections to V1 would take at least 100 ms. Given that hierarchical models of the visual system cannot explain such small timing differences here reported between V1 and MT, it is likely that the fastest responses that we observed in MT are not dependent on V1 input. Rather, we propose a V1-bypassing circuit, which sustains early motion perception responsible for the shift when coding the position of stationary objects. In this sense, the fast visual inputs that MT receives from the superior colliculus (SC) through the pulvinar, as well as the direct route from the lateral geniculate nucleus (LGN), might arise as better candidates to be the anatomical basis of the first stages of this phenomenon. Although there is some controversy about the latency of SC-pulvinar inputs to MT—from 40 ms (ffytche et al., 1995) to 90 ms (Schoenfeld et al., 2002)—this secondary visual pathway has continuously generated interest as a potential source of visual motion inputs to MT. Recent clinical and neuroanatomical studies have sought evidence that retinocollicular pathways to high order dorsal stream areas, such as those to MT, may explain motion discrimination in the absence of V1 (Azzopardi & Hock, 2011; Lyon, Nassi, & Callaway, 2010). Since a reliable group of retinal projections terminates directly in the pulvinar (O'Brien, Abel, & Olavarria, 2001), the functional significance of this considerably direct pathway to MT might mediate the fast transmission of feedforward retinal inputs to higher-order areas of the dorsal stream. However, a recent study has cast doubts on the pulvinar as a powerful source of motion inputs to MT (Berman & Wurtz, 2011), proposing instead the direct path from LGN to MT as the most straightforward explanation for motion perception when V1 is impaired. This account is based on the suppression of MT activity during LGN blockade (Maunsell, Nealey, & DePriest, 1990; Schmid et al., 2010). All in all, the functional role of MT motion inputs from LGN and SC pulvinar pathways remains to be elucidated.

Some issues need to be addressed in future studies. First, our results do not discriminate the underlying component of motion responsible for the motion-induced hand shift. Further psychophysical studies may address this question using a temporal flicker to disentangle the effect of motion speed and temporal frequency. A second limitation relies on which secondary visual pathway conveys the motion signals that posteriorly cause the shift. This question could be tackled with neuroanatomical recordings in conjunction with effective comparisons of the deficits in motion perception caused by the independent disruption of LGN and pulvinar. Finally, a technical constraint of our study concerns the low spatial resolution that EEG entails for source localization. With our approach, we were able to establish a very precise temporal cutoff between the neural activity that can be attributed to V1-dependent visual pathways or to nonprimary visual pathways. However, the current arrangement of electrodes used to implement CSD transformation is not optimal, and can hardly distinguish which extrastriate region of the visual cortex sustains the source activity. It is likely, however, that further imaging studies help to clarify the specific extrastriate locus that actively contributes to the motion-induced mislocalization of objects.

## References


Akaike, H. (1974). A new look at the statistical model identification. *IEEE Transactions on Automatic Control*, *19*, 716–723. doi: 10.1109/TAC.1974.1100705

Azzopardi, P., & Hock, H. S. (2011). Illusory motion perception in blindsight. *Proceedings of the National Academy of Sciences of the United States of America*, *108*, 876–881. doi: 10.1073/pnas.1005974108

Barbur, J. L., Watson, J. D., Frackowiak, R. S., & Zeki, S. (1993). Conscious visual perception without V1. *Brain*, *116*(Pt 6), 1293–1302. doi: 10.1093/brain/116.6.1293

Bartsch, M. V., Boehler, C. N., Stoppel, C. M., Merkel, C., Heinze, H. J., Schoenfeld, M. A., & Hopf, J. M. (2014). Determinants of global color-based selection in human visual cortex. *Cerebral Cortex*. Advance online publication. doi: 10.1093/cercor/bhu078

Berman, R. A., & Wurtz, R. H. (2011). Signals conveyed in the pulvinar pathway from superior colliculus to cortical area MT. *Journal of Neuroscience*, *31*, 373–384. doi: 10.1523/JNEUROSCI.4738-10.2011

Berry, M. J., Brivanlou, I. H., Jordan, T. A., & Meister, M. (1999). Anticipation of moving stimuli by the retina. *Nature*, *398*, 334–338. doi: 10.1038/18678

Bock, O. (1986). Contribution of retinal versus extraretinal signals towards visual localization in goal-directed movements. *Experimental Brain Research*, *64*, 476–482. doi: 10.1007/BF00340484

Brenner, E., & Smeets, J. B. (1997). Fast responses of the human hand to changes in target position. *Journal of Motor Behavior*, *29*, 297–310. doi: 10.1080/00222899709600017

Buchner, H., Gobbele, R., Wagner, M., Fuchs, M., Waberski, T. D., & Beckmann, R. (1997). Fast visual evoked potential input into human area V5. *NeuroReport*, *8*, 2419–2422. doi: 10.1097/00001756-199707280-00002

Burr, D. C. (1981). Temporal summation of moving images by the human visual system. *Proceedings of the Royal Society of London. Series B: Biological Sciences*, *211*, 321–339. doi: 10.1098/rspb.1981.0010

Cai, R. H., Pouget, A., Schlag-Rey, M., & Schlag, J. (1997). Perceived geometrical relationships affected by eye-movement signals. *Nature*, *386*, 601–604. doi: 10.1038/386601a0

Clark, V. P., Fan, S., & Hillyard, S. A. (1994). Identification of early visual evoked potential generators by retinotopic and topographic analyses. *Human Brain Mapping*, *2*, 170–187. doi: 10.1002/hbm.460020306

Cunillera, T., Gomila, A., & Rodriguez-Fornells, A. (2008). Beneficial effects of word final stress in segmenting a new language: Evidence from ERPs. *BMC Neuroscience*, *9*, 1–10. doi: 10.1186/1471-2202-9-23

Cunillera, T., Toro, J. M., Sebastian-Galles, N., & Rodriguez-Fornells, A. (2006). The effects of stress and statistical cues on continuous speech segmentation: An event-related brain potential study. *Brain Research*, *1123*, 168–178. doi: 10.1016/j.brainres.2006.09.046

De Valois, R. L., & De Valois, K. K. (1991). Vernier acuity with stationary moving Gabors. *Vision Research*, *31*, 1619–1626. doi: 10.1016/0042-6989(91)90138-U

de'Sperati, C., & Baud-Bovy, G. (2008). Blind saccades: An asynchrony between seeing and looking. *Journal of Neuroscience*, *28*, 4317–4321. doi: 10.1523/JNEUROSCI.0352-08.2008

Durant, S., & Johnston, A. (2004). Temporal dependence of local motion induced shifts in perceived position. *Vision Research*, *44*, 357–366. doi: 10.1016/j.visres.2003.09.022

ffytche, D. H., Guy, C. N., & Zeki, S. (1995). The parallel visual motion inputs into areas V1 and V5 of human cerebral cortex. *Brain*, *118*(Pt 6), 1375–1394. doi: 10.1093/brain/118.6.1375

Fu, Y. X., Shen, Y., Gao, H., & Dan, Y. (2004). Asymmetry in visual cortical circuits underlying motion-induced perceptual mislocalization. *Journal of Neuroscience*, *24*, 2165–2171. doi: 10.1523/JNEUROSCI.5145-03.2004

Fukiage, T., Whitney, D., & Murakami, I. (2011). A flash-drag effect in random motion reveals involvement of preattentive motion processing. *Journal of Vision*, *11*. doi: 10.1167/11.13.12

Gomi, H., Abekawa, N., & Nishida, S. (2006). Spatiotemporal tuning of rapid interactions between visual-motion analysis and reaching movement. *Journal of Neuroscience*, *26*, 5301–5308. doi: 10.1523/JNEUROSCI.0340-06.2006

Granger, C. W. (1969). Investigating causal relations by econometric models and cross-spectral methods. *Econometrica*, 424–438. doi: 10.1017/CBO9780511753978.002

Hesse, W., Moller, E., Arnold, M., & Schack, B. (2003). The use of time-variant EEG Granger causality for inspecting directed interdependencies of neural assemblies. *Journal of Neuroscience Methods*, *124*, 27–44. doi: 10.1016/S0165-0270(02)00366-7

Jancke, D., Erlhagen, W., Schoner, G., & Dinse, H. R. (2004). Shorter latencies for motion trajectories than for flashes in population responses of cat primary visual cortex. *Journal of Physiology*, *556*, 971–982. doi: 10.1113/jphysiol.2003.058941

Jennings, J. R., & Wood, C. C. (1976). Letter: The epsilon-adjustment procedure for repeated-measures analyses of variance. *Psychophysiology*, *13*, 277–278. doi: 10.1111/j.1469-8986.1976.tb00116.x

Klein, C., Andresen, B., Berg, P., Kruger, H., & Rockstroh, B. (1998). Topography of CNV and PINV in schizotypal personality. *Psychophysiology*, *35*, 272–282. doi: 10.1017/S0048577298961212

Kuba, M., Toyonaga, N., & Kubova, Z. (1992). Motion-reversal visual evoked responses. *Physiological Research*, *41*, 369–373.

Kwiatkowski, D., Phillips, P. C., Schmidt, P., & Shin, Y. (1992). Testing the null hypothesis of stationarity against the alternative of a unit root: How sure are we that economic time series have a unit root? *Journal of Econometrics*, *54*, 159–178. doi: 10.1016/0304-4076(92)90104-Y

Lyon, D. C., Nassi, J. J., & Callaway, E. M. (2010). A disynaptic relay from superior colliculus to dorsal stream visual cortex in macaque monkey. *Neuron*, *65*, 270–279. doi: 10.1016/j.neuron.2010.01.003

Maunsell, J. H. (1987). Physiological evidence for two visual subsystems. *Matters of Intelligence* (pp. 59–87). Amsterdam, The Netherlands: Springer.

Maunsell, J. H., Nealey, T. A., & DePriest, D. D. (1990). Magnocellular and parvocellular contributions to responses in the middle temporal visual area (MT) of the macaque monkey. *Journal of Neuroscience*, *10*, 3323–3334.

Maus, G. W., Fischer, J., & Whitney, D. (2013). Motion-dependent representation of space in area MT+. *Neuron*, *78*, 554–562. doi: 10.1016/j.neuron.2013.03.010

McCarthy, G., & Wood, C. C. (1985). Scalp distributions of event-related potentials: An ambiguity associated with analysis of variance models. *Electroencephalography and Clinical Neurophysiology*, *62*, 203–208. doi: 10.1016/0168-5597(85)90015-2

McGraw, P. V., Walsh, V., & Barrett, B. T. (2004). Motion-sensitive neurones in V5/MT modulate perceived spatial position. *Current Biology*, *14*, 1090–1093. doi: 10.1016/j.cub.2004.06.028

Mitzdorf, U. (1985). Current source-density method and application in cat cerebral cortex: Investigation of evoked potentials and EEG phenomena. *Physiological Reviews*, *65*, 37–100.

Mohrmann-Lendla, H., & Fleischer, A. G. (1991). The effect of a moving background on aimed hand movements. *Ergonomics*, *34*, 353–364. doi: 10.1080/00140139108967319

Murakami, I. (2001). The flash-lag effect as a spatiotemporal correlation structure. *Journal of Vision*, *1*, 126–136. doi: 10:1167/1.2.6

Neggers, S. F., & Bekkering, H. (2002). Coordinated control of eye and hand movements in dynamic reaching. *Human Movement Science*, *21*, 349–376. doi: 10.1016/S0167-9457(02)00120-3

Nijhawan, R. (2002). Neural delays, visual motion and the flash-lag effect. *Trends in Cognitive Science*, *6*, 387–393. doi: 10.1016/S1364-6613(02)01963-0

Nishida, S., & Johnston, A. (1999). Influence of motion signals on the perceived position of spatial pattern. *Nature*, *397*, 610–612. doi: 10.1038/17600

Nowak, L. G., & Bullier, J. (1997). The timing of information transfer in the visual system. *Cerebral Cortex*, *12*, 205–242. doi: 10.1007/978-1-4757-9625-4_5

Nunez, P. L. (2006). *Electric fields of the brain: The neurophysics of EEG*. Oxford, UK: Oxford University Press.

O'Brien, B. J., Abel, P. L., & Olavarria, J. F. (2001). The retinal input to calbindin-D28k-defined subdivisions in macaque inferior pulvinar. *Neuroscience Letters*, *312*, 145–148. doi: 10.1016/S0304-3940(01)02220-0

Perenin, M., & Jeannerod, M. (1975). Residual vision in cortically blind hemiphields. *Neuropsychologia*, *13*, 1–7. doi: 10.1016/0028-3932(75)90041-X

Perrin, F., Pernier, J., Bertrand, O., & Echallier, J. F. (1989). Spherical splines for scalp potential and current density mapping. *Electroencephalography and Clinical Neurophysiology*, *72*, 184–187. doi: 10.1016/0013-4694(89)90180-6

Purushothaman, G., Patel, S. S., Bedell, H. E., & Ogmen, H. (1998). Moving ahead through differential visual latency. *Nature*, *396*, 424. doi: 10.1038/24766.

Rodionov, V., Goodman, C., Fisher, L., Rosenstein, G. Z., & Sohmer, H. (2002). A new technique for the analysis of background and evoked EEG activity: Time and amplitude distributions of the EEG deflections. *Clinical Neurophysiology*, *113*, 1412–1422. doi: 10.1016/S1388-2457(02)00199-2

Rodriguez-Herreros, B., & Lopez-Moliner, J. (2008). The influence of motion signals in hand movements. *Experimental Brain Research*, *191*, 321–329. doi: 10.1007/s00221-008-1527-1

Saijo, N., Murakami, I., Nishida, S., & Gomi, H. (2005). Large-field visual motion directly induces an involuntary rapid manual following response. *Journal of Neuroscience*, *25*, 4941–4951. doi: 10.1523/JNEUROSCI.4143-04.2005

Scherg, M. (1990). Fundamentals of dipole source potential analysis. *Auditory Evoked Magnetic Fields and Electric Potentials. Advances in Audiology*, *6*, 40–69. doi: 10.1016/j.bspc.2015.01.004

Schmid, M. C., Mrowka, S. W., Turchi, J., Saunders, R. C., Wilke, M., Peters, A. J., . . . Leopold, D. A. (2010). Blindsight depends on the lateral geniculate nucleus. *Nature*, *466*, 373–377. doi: 10.1038/nature09179

Schmolesky, M. T., Wang, Y., Hanes, D. P., Thompson, K. G., Leutgeb, S., Schall, J. D., & Leventhal, A. G. (1998). Signal timing across the macaque visual system. *Journal of Neurophysiology*, *79*, 3272–3278.

Schneider, M. R. (1972). A multistage process for computing virtual dipolar sources of EEG discharges from surface information. *IEEE Transactions on Biomedical Engineering*, *19*, 1–12. doi: 10.1109/TBME.1972.324152

Schoenfeld, M. A., Noesselt, T., Poggel, D., Tempelmann, C., Hopf, J. M., Woldorff, M. G., . . . Hillyard, S. A. (2002). Analysis of pathways mediating preserved vision after striate cortex lesions. *Annals of Neurology*, *52*, 814–824. doi: 10.1002/ana.10394

Seth, A. K. (2010). A MATLAB toolbox for Granger causal connectivity analysis. *Journal of Neuroscience Methods*, *186*, 262–273. doi: 10.1016/j.jneumeth.2009.11.020

Shipp, S., & Zeki, S. (1989). The organization of connections between areas V5 and V1 in macaque monkey visual cortex. *European Journal of Neuroscience*, *1*, 309–332. doi: 10.1111/j.1460-9568.1989.tb00798.x

Sincich, L. C., Park, K. F., Wohlgemuth, M. J., & Horton, J. C. (2004). Bypassing V1: A direct geniculate input to area MT. *Nature Neuroscience*, *7*, 1123–1128. doi: 10.1038/nn1318

Snowden, R. J. (1998). Shifts in perceived position following adaptation to visual motion. *Current Biology*, *8*, 1343–1345. doi: 10.1016/S0960-9822(07)00567-2

Standage, G. P., & Benevento, L. A. (1983). The organization of connections between the pulvinar and visual area MT in the macaque monkey. *Brain Research*, *262*, 288–294. doi: 10.1016/0006-8993(83)91020-X

Steinman, R. M., Kowler, E., & Collewijn, H. (1990). New directions for oculomotor research. *Vision Research*, *30*, 1845–1864. doi: 10.1016/0042-6989(90)90163-F

Stevens, M. C., Calhoun, V. D., & Kiehl, K. A. (2005). Hemispheric differences in hemodynamics elicited by auditory oddball stimuli. *NeuroImage*, *26*, 782–792. doi: 10.1016/j.neuroimage.2005.02.044

Sundberg, K. A., Fallah, M., & Reynolds, J. H. (2006). A motion-dependent distortion of retinotopy in area V4. *Neuron*, *49*, 447–457. doi: 10.1016/j.neuron.2005.12.023

Talairach, J., & Tournoux, P. (1988). *Co-planar stereotaxic atlas of the human brain. 3-Dimensional proportional system: An approach to cerebral imaging*. Stuttgart, Germany: Thieme.

Tse, P. U., Whitney, D., Anstis, S., & Cavanagh, P. (2011). Voluntary attention modulates motion-induced mislocalization. *Journal of Vision*, *11*, 12. doi: 10.1167/11.3.12

van Beers, R. J., Haggard, P., & Wolpert, D. M. (2004). The role of execution noise in movement variability. *Journal of Neurophysiology*, *91*, 1050–1063. doi: 10.1152/jn.00652.2003

Vetter, P., Grosbras, M. H., & Muckli, L. (2013). TMS Over V5 disrupts motion prediction. *Cerebral Cortex*, *25*, 1052–1059. doi: 10.1093/cercor/bht297

Wang, X., Chen, Y., & Ding, M. (2008). Estimating Granger causality after stimulus onset: A cautionary note. *NeuroImage*, *41*, 767–776. doi: 10.1016/j.neuroimage.2008.03.025

Whitney, D., & Cavanagh, P. (2000). Motion distorts visual space: Shifting the perceived position of remote stationary objects. *Nature Neuroscience*, *3*, 954–959. doi: 10.1038/78878

Whitney, D., Ellison, A., Rice, N. J., Arnold, D., Goodale, M., Walsh, V., & Milner, D. (2007). Visually guided reaching depends on motion area MT+. *Cerebral Cortex*, *17*, 2644–2649. doi: 10.1093/cercor/bhl172.

Whitney, D., Goltz, H. C., Thomas, C. G., Gati, J. S., Menon, R. S., & Goodale, M. A. (2003). Flexible retinotopy: Motion-dependent position coding in the visual cortex. *Science*, *302*, 878–881. doi: 10.1126/science.1087839

Whitney, D., Westwood, D. A., & Goodale, M. A. (2003). The influence of visual motion on fast reaching movements to a stationary object. *Nature*, *423*, 869–873. doi: 10.1038/nature01693

Wojtach, W. T., Sung, K., Truong, S., & Purves, D. (2008). An empirical explanation of the flash-lag effect. *Proceedings of the National Academy of Sciences of the United States of America*, *105*, 16338–16343. doi: 10.1073/pnas.0808916105

Zhang, Y., & Ding, M. (2010). Detection of a weak somatosensory stimulus: Role of the prestimulus mu rhythm and its top-down modulation. *Journal of Cognitive Neuroscience*, *22*, 307–322. doi: 10.1162/jocn.2009.21247

(Received January 15, 2015; Accepted July 27, 2015)